Synthesis, characterization and bioactivity of a glass/acrylic bone cement composite

J. SIMITZIS, D. E. BACIU*
National Technical University of Athens, School of Chemical Engineering, Department III "Materials Science and Engineering", Laboratory Unit "Advanced and Composite Materials", 9 Heroon Polytechniou str., Zografou Campus, 157 73 Athens, Greece

Bioactive bone cement composite was prepared by mixing beads of PMMA, methylmethacrylate monomer, benzoyl peroxide as free radical initiator and bioglass powder. The latter consisted of SiO_2, CaO and P_2O_5 was produced by the sol-gel method. The structure of PMMA beads, glasses and bone cement composite were investigated by TG/DTG, FTIR, XRD and SEM/EDS. The in vitro bioactivity was carried out by immersing specimens of the cement composite in simulated body fluid (SBF) at 37 ^{0}C and pH 7.4 for a reaction time period of 14 days.

(Received March 26, 2012; accepted June 6, 2012)

Keywords: PMMA, bone cements, bioglasses, TG/DTG, SEM/EDS

1. Introduction

Over the last 5 years the bone cement materials become one of the major fields in biomaterials. Bone cements are materials employed in orthopaedic surgery and dental applications for the fixation of joints prosthesis to act as a load distributor between the artificial implant and the bone, as well as filling selfcuring materials for bone and dental cavities [1]. The most widely used bone cement is based on polymethylmethacrylate (PMMA), also called acrylic bone cement. PMMA is used in clinical applications to fix joint prostheses for hip and knee joints [2, 3]. Approximately 50% of all orthopedic implants utilize bone cement to achieve implant fixation. However, local tissue damage due to chemical reactions during polymerization, the high shrinkage of the cement after polymerization, the stiffness mismatch between the bone and the cement are some drawbacks associated with PMMA-based bone cements. Loose cement particles also mediate osteolysis of the bone. Loosening is recognized as one of the primary sources of total hip replacement failure [4]. Several investigators have been researching alternative formulations to improve the deficiencies noted above. Bioactive bone cements including calcium phosphate cements and polymeric cements with bioactive fillers have been reported as alternatives to acrylic bone cements. The rationale of the inclusion of a bioactive phase is attractive due to its bone bonding ability and combination of properties of different phases [5].

In this work, a bioactive bone cement composite was prepared by mixing beads of PMMA (produced by suspension polymerization), methylmethacrylate (MMA) monomer, benzoyl peroxide (BPO) as free radical initiator and bioglass powder. The latter consisted of SiO_2, CaO and P_2O_5 was produced by the sol-gel method with initial molar proportion of $SiO_2/CaO/P_2O_5$=50:45:5 [6, 7]. Bioactivation of the PMMA bone cement by adding bioglass powder can be an advantageous solution for problems of bone filling as well as bone regeneration and may also strengthen bone-cement interface.

2. Experimental

2.1. Preparation of bioactive glasses

The bioglass based on SiO_2, CaO and P_2O_5 was produced by the sol-gel method with initial molar proportion of $SiO_2/CaO/P_2O_5$ = 50:45:5. The procedure was similar to that of Hench and Saravanapavan [6, 7]. The sol was prepared by mixing distilled water, HNO_3, tetraethyl orthosilicate (TEOS), triethyl phosphate (TEP) and calcium nitrate tetrahydrate $Ca(NO_3)_2.4H_2O$, following this order. The liquid remained in a small cylindrical bottle which was hermetically closed with its lid and left to gel at room temperature for 4 days. The bottle was transferred without its lid to an oven and heated at 60 ^{0}C, for 3 days in order to age the gel. Then, it followed the drying at 150 ^{0}C for 2 days. The dried gel was thermally stabilized in an electric furnace at 700 ^{0}C for 3 hours under air atmosphere. The stabilized glass was ground and sieved and the portion of grains less than 63 μm was used.

The structure of the bioactive glasses was investigated by Fourier transform infrared spectroscopy (FTIR), thermogravimetric and differential thermal analysis (TG/DTG), and X-ray diffraction (XRD).

2.2. Preparation of PMMA beads

PMMA beads were prepared by free radical suspension polymerization [8]. The raw materials: water, suspending agent (CMC), monomer (MMA) and initiator (BPO) were added in a 1L three-necked reactor equipped with a reflux condenser, a mechanical stirrer and a temperature control system. The polymer was received as beads and after sieving its portion less than 100 μm was used.

The produced PMMA was characterized by FTIR, and scanning electron microscopy (SEM).

2.3. Preparation of glass/acrylic bone cement composite

The glass/ acrylic bone cement composite was prepared as follows:

Bioglass powder (4 g) was added to a solution of PMMA beads (2 g) in MMA (4 ml) with benzoyl peroxide (BPO) as free radical initiator (0.5 wt %). The components of bone cement composite were hand-mixed for ca. 5 min until the mixture became a paste with high viscosity. Then, the paste was placed into bar-shaped molds. The polymerization mixture was carried out in at 60 ^{0}C for 24 hours.

The structure of the glass/acrylic bone cement composite was investigated by FTIR, TG/DTG, XRD and SEM/EDS.

Characterization of the materials by FTIR, TG/DTG, XRD, SEM/EDS.

FTIR spectra were recorded using a Perkin Elmer Spectrum 2000, on discs prepared by mixing of the sample powder and KBr.

TG/DTG curves were recorded using a TG/STDA Mettler Toledo 851 instrument. The sample was heated from 25 to 1300 ^{0}C at a constant heating rate of 5 ^{0}C/min under air atmosphere.

XRD measurements were performed with a Siemens D5000 X-Ray Diffractometer by using sample of the material as powder.

The SEM-EDS studies were carried out in a FEI Quanta 200 Scanning Electron Microscope (SEM) and simultaneously elemental analysis was determined by Energy Dispersive Spectroscopy (EDS). The material was examined as specimen with dimensions of 10x8x4mm.

2.4. Characterization of the cement composite by "in vitro" study

The in vitro bioactivity of the cement composite was carried out by immersing specimens with dimensions of 10x8x4 mm in 50 ml simulated body fluid (SBF), as has been proposed by Kokubo [9], at 37 ^{0}C and pH 7.4 for a reaction time period of 14 days. Then, the surface of the cement composite was studied by FTIR, XRD and SEM/EDS.

3. Results and discussion

3.1. Bioactive glasses- results FTIR

Fig. 1 shows the FTIR spectra of the glass after aging, drying and stabilization.

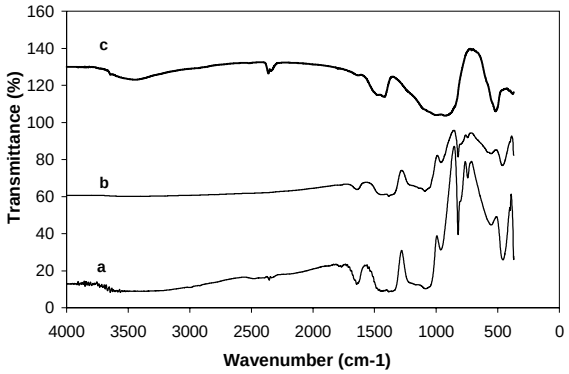

Fig. 1. FTIR spectra of the glass after (a) aging at 60 ^{0}C (b) drying at 120 ^{0}C; (c) stabilization at 700 ^{0}C.

According to the *Fig. 1* (a), the peak at 471 cm^{-1} is assigned to the bending modes of the Si-O-Si and O-Si-O bonds [6, 10]. A doublet at 546, 599 cm^{-1} is associated with the O–P–O stretching vibrations of phosphate groups [14]. The peak at 811cm^{-1} corresponds to the stretching mode of the O-Si-O bond [6, 10, 12]. The peak at 954 cm^{-1} corresponds to the Si-O-Ca bonds containing non-bridging oxygen [6, 13]. The peak at 1086cm^{-1} is attributed to the symmetric stretching vibration of the Si-O-Si bonds [6, 12]. The peak at 1379 cm^{-1} is assigned to the vibration of ionic $(NO_3)^-$ [6, 10, 12]. The vibration of H_2O (vibration due to the OH bond) is at 1633 cm^{-1} [6, 12]. No peaks assigned to organic matter have been observed.

The same bands are observed for the dried glass (Fig.1 (b)).

According to the Fig. *1 (c)*, after the stabilization at 700 ^{0}C, the material shows the peaks of H_2O (vibration due to the OH bond), Si-O-Si and O-Si-O (bending modes), O-Si-O (stretching modes) and Si-O-Si (symmetric stretching modes). The peak at 1380 cm^{-1} due to the vibration of ionic $(NO_3)^-$ is disappeared [6, 10, 12]. According to literature, the peak at 1414 cm^{-1} corresponds to $(CO_3)^{2-}$ groups [14]. The presence of carbonate is attributed to a carbonation process of the material due to the atmospheric CO_2 as a consequence of the high calcium content [14].

TG/DTG

Fig. 2 and 3 shows the TGA /DTG curves of the glasses after drying and stabilization, respectively.

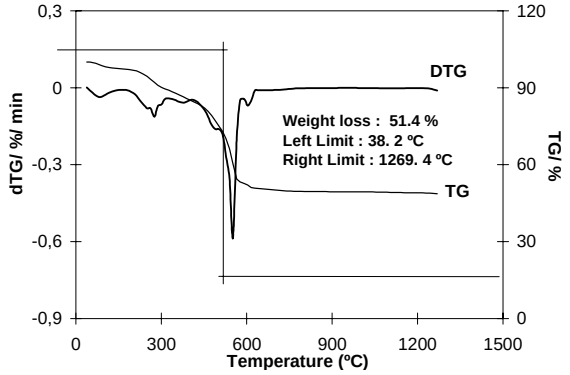

Fig. 2. TG/DTG curves of the glass after drying at 150 ^{0}C.

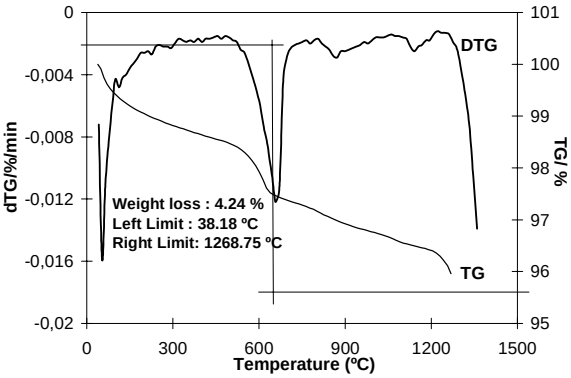

Fig.3. TG/DTG curves of the glass after stabilization at 700 ^{0}C.

According to the *Fig. 2* the dried material at 150 ^{0}C during its thermal treatment up to 1300 ^{0}C exhibits the following weight losses: 2.8 % up to 175 ^{0}C, 8.2 % between 175 - 326 ^{0}C, 38.1 % between 326 -641 ^{0}C and 2.1 % between 641 and 1300 ^{0}C, i.e. the total weight loss is approx. 51.2 %. The weight loss up to 326 ^{0}C is attributed to the loss of residual water and ethanol [6, 10] and that between 326 - 641 ^{0}C to the loss of organic (i.e. alkoxy group) and nitrates (in the form of $CaNO_3.4H_2O$ and HNO_3) used in the sol preparation [10, 11].

According to the *Fig. 3*, the stabilized material at 700 ^{0}C during its thermal treatment up to 1200 ^{0}C exhibits the following weight losses: 1.4 % up to 450 ^{0}C, 1.2 % between 450 - 713 ^{0}C and 1.05 % between 713 - 1200 ^{0}C, i.e. the total weight loss is approx. 3.6 %. The weight loss up to 450 ^{0}C is attributed to the loss of residual water and ethanol [6, 10] and that between 450 - 713 ^{0}C to the loss of organic (i.e. alkoxy group) and nitrates (in the form of $CaNO_3.4H_2O$ and HNO_3) used in the sol preparation [10, 11].

XRD

Fig. 4 shows the XRD results of the glass after the thermal process at 700 ^{0}C. The diffractogram has no reflection and its form indicates internal disorder i.e. an amorphous state of the glass as it was expected.

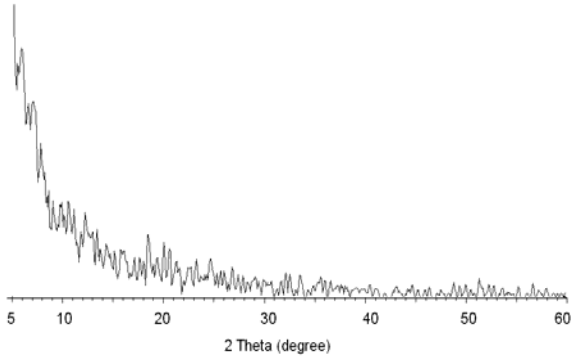

Fig. 4. XRD diffractogram of the glass after thermal process at 700 ^{0}C.

3.2. PMMA- results

FTIR

Fig. 5 shows the FTIR spectrum of the PMMA.

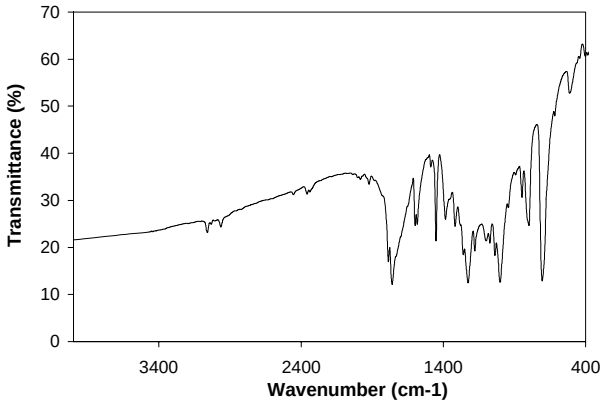

Fig. 5. FTIR spectrum of PMMA.

The characteristic vibration bands of PMMA appear at 1751 cm^{-1} ν(C=O) and 1451cm^{-1} ν(C–O). The bands at 3054 and 2958 cm^{-1} correspond to the C–H stretching of the methyl group (CH_3) and the bands at 1315 and 1451 cm^{-1} are associated with C–H symmetric and asymmetric stretching modes, respectively. The 1244 cm^{-1} band is assigned to torsion of the methylene group (CH_2) and the 1176 cm^{-1} band corresponds to vibration of the ester group C–O, while C–C stretching bands are at 997 and 845 cm^{-1} [15, 16, 17].

SEM

Fig. 6 shows the SEM image of PMMA beads. As clearly seen, the PMMA beads have a spherical form. The diameter of the most beads is approx. 32 μm.

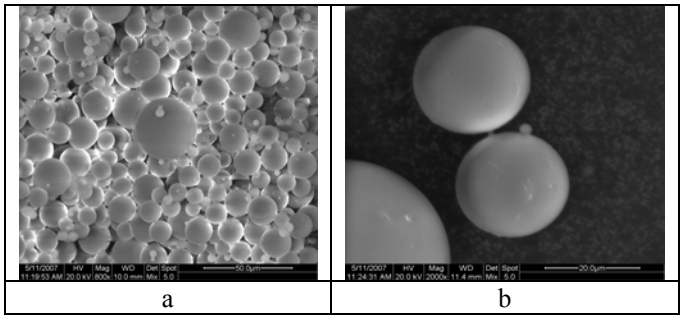

Fig. 6. SEM image of PMMA beads: (a) magnification 800x; (b) magnification 2000x.

3.3 Bone cement composite- results

FTIR

Fig. 7 shows the FTIR spectra of the bone cement composite before and after 14 days immersion in SBF.

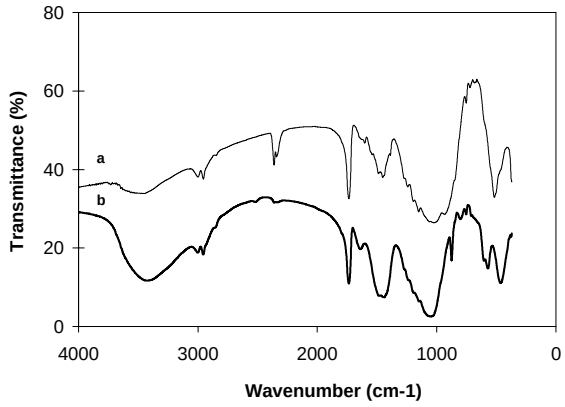

Fig. 7. FTIR spectra of the bone cement composite (a) before and (b) after 14 days immersion in SBF.

According to the literature, the peaks at 563-593, 955 and 1035 cm^{-1} are assigned to the (P-O) vibrational mode of an amorphous phosphate [10]. According to the literature, the peaks at 1428, 1470 and 872 cm^{-1} correspond to (CO_3^{2-}) carbonate group [10].

TG/DTG

Fig. 8 shows the TGA /DTG curves of the bone cement composite after polymerization at 60 ^{0}C for 1 day.

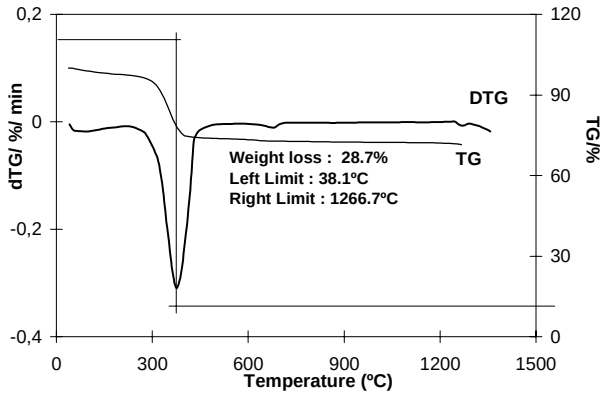

Fig.8. TG/DTG curves of the bone cement composite.

According to the literature, the weight loss of 28.77% between 240 and 430 ^{0}C corresponds with the PMMA decomposition [18].

XRD

The XRD results of the bone cement composite show XRD patterns typical of amorphous materials. Fig. 9 shows the XRD results of the bone cement composite.

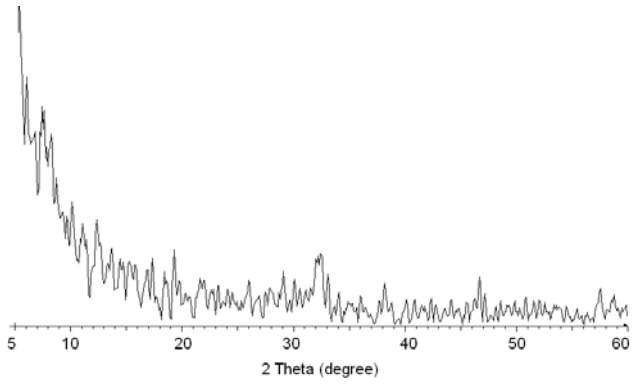

Fig. 9. XRD diffractogram of the bone cement composite.

3.4. In vitro bioactivity study of the bone cement composite- results

XRD

Fig. 10 shows the XRD diffractogram of the bone cement composite before and after 14 days immersion in SBF.

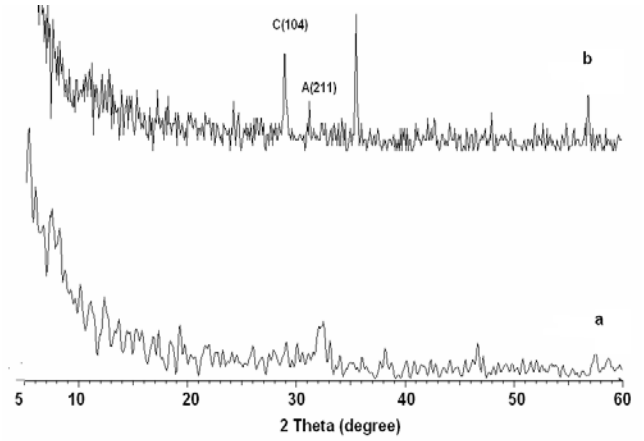

Fig. 10. XRD diffractogram of the bone cement composite (a) before and (b) after 14 days immersion in SBF.

XRD patterns of the bone cement composites before immersion in SBF solution show that it is an amorphous material. When the bone cement composite is in contact with SBF for 14 days (Fig. 10), the XRD diffractogram indicates the formation of two phases: (211) of apatite and (104) of calcite with a larger proportion of the calcite phase [12].

SEM/EDS

SEM/EDS studies obtained from bone cement composite before and after the immersion in SBF solution are shown in the Fig. 11(a), (b); Fig. 12(a1), (a2), (b) and Fig. 13(a), (b). According to the Fig. 11 (a), the surface of the bone cement composite before the immersion in SBF solution is heterogenous. After 14 day's immersion in SBF solution the surface of the bone cement composite has been covered by clear shaped rounded aggregated (HA) particles as shown in the Fig. 12 (a1), (a2). According to the Fig. 12 (b), the EDS results reveal the inclusion of the phosphorous in the composition of the newly formed layer. The crystallized apatite layer contains also minor components such as Na, Cl, and Mg and the Ca/P atomic ratio was 1.62, which was close to the theoretical value of 1.67 for apatite ($Ca_{10}(PO_4)_6(OH)_2$) [19]. It can be observed by SEM photograph as shown in the Fig. 13 (a), (b) that the apatite layer does not grow only on the external surface of the composite, but also inside the material, where big pores exist. According to the literature, a high concentration of Ca^{2+} is released through the pores leading to the apatite growth, similar to the way that it is produced on the external surface [18].

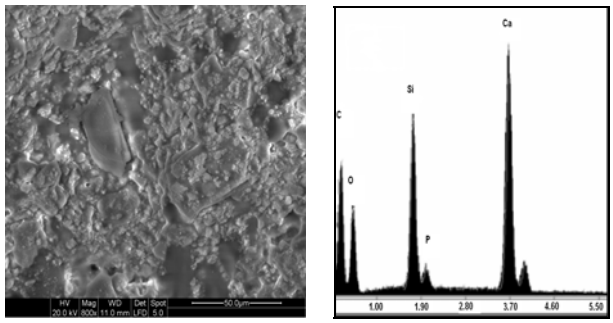

a b

Fig. 11. (a) SEM image (magnification 800x) and (b) EDS spectrum of the bone cement composite surface, before the immersion in SBF solution.

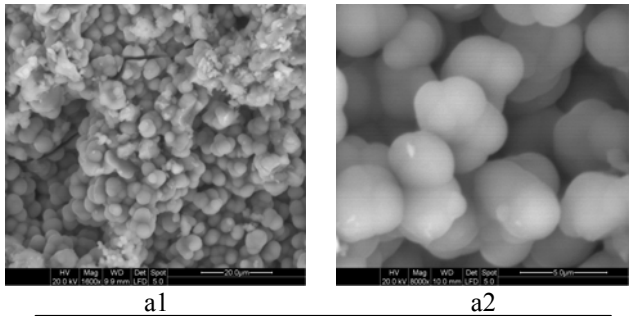

a1 a2

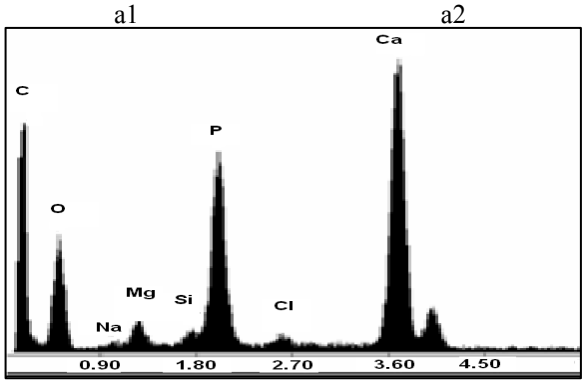

b

Fig. 12. (a1) SEM image (clear shaped rounded aggregated HA particles) magnification 1600x; (a2) magnification 800x and (b) EDS spectrum of the bone cement composite surface, after 14 days immersion in SBF.

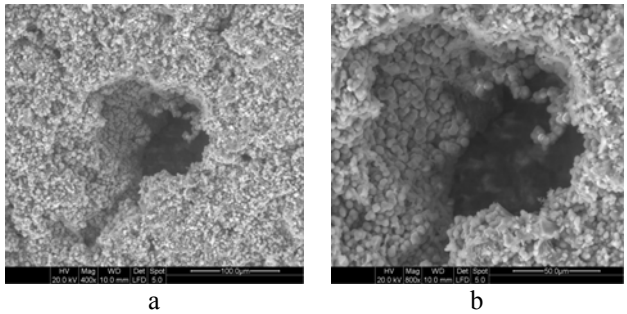

a b

Fig. 13. SEM image of the bone cement composite after 14 days immersion in SBF. A big pore covered by a new grown phase; (a) magnification 400x and (b) magnification 800x.

To replace a PMMA bone cement with a bioactive cement, it should have similar handling properties, better mechanical properties and high osteoconductivity. Adding a bioactive glass filler (which has high ability to bond directly to bone through an apatite layer) [12] would strengthen bone-cement interface which is considered a weak point in bone-cement implant construct. According to the literature reinforcing the PMMA cement with bioactive filler reduces the amount of added monomer, leading to a decrease of exotherm during the polymerization, decrease of polymerization shrinkage and increase of mechanical properties of the cement [20].

In this work, the bioglass prepared by sol-gel method is amorphous, homogenous with high purity and after stabilization at 700 ^{0}C. No traces of organic matter or nitrates in the stabilized biomaterial were found according to FTIR and TG/DTA analysis.

The PMMA beads obtained by suspension polymerization have particles size <100 μm. The SEM images show clearly their spherical form and rough surface. According to previous reports using small-diameter PMMA beads improves the handling properties, the mechanical properties of the PMMA –based cements [20].

The glass /acrylic bone cement composite obtained has excellent bioactivity. After 14 day's immersion in SBF solution the surface of the bone cement composite has been covered by clear shaped rounded aggregated (HA) particles. The Ca/P atomic ratio was 1.62, which was close to the theoretical value of 1.67 for apatite ($Ca_{10}(PO_4)_6(OH)_2$) [18]. The SEM results reveal that the apatite layer does not grow only on the external surface of the composite, but also inside the material, where big pores exist.

FTIR data together with the XRD patterns confirms that a hydroxycarbonate apatite (HCA) layer grows on the surface of the glass/acrylic bone cement composite.

4. Conclusions

It can be concluded that a suitable glass/acrylic bone cement composite have been synthesized which can be used as biomaterial candidate. Bioactivation of the PMMA bone cement by adding bioglass powder can be an advantageous solution for problems of bone filling as well as bone regeneration.

Acknowledgements

The authors gratefully acknowledge Mr. Loukas Zoumpoulakis, Assistant Professor in the School of Chemical Engineering, Department of Materials Science and Engineering, National Technical University of Athens, for his technical collaboration. Also, the authors would like to thank Prof. A. Vgenopoulos of the School of Mining Engineering and Metallurgy, for kindly helping for FTIR measurements.

References

[1] Espigares, C. Elvira, J. F. Mano, B. Vazquez, J. S. Roman, R. L. Reis, Biomaterials **23**, 1883 (2002).
[2] S. Ramakrishna, J. Mayer, E. Wintermantel, Kam W. Leong, Composites Science and Technology **61**, 1189 (2001).
[3] T.Yamamuro, T. Nakamura, M.Iida, K. Kawanabe, Y. Matsuda, K. Ido, J. Tamura, Y. Senaha, Biomaterials **19**, 1479 (1998).
[4] F. Zivic, M. Babic, N. Grujovic, S. Mitrovic, G. Favaro, M. Caunii, Journal of the mechanical behavior of biomedical materials **5**, 129 (2012).
[6] S. Deb, L. Aiyathurai, J. A. Roether, Z. B. Luklinska, Biomaterials **26**, 3713 (2005).
[7] P. Saravanapavan, Larry. L. Hench, Journal of Non-Crystalline Solids **318**, 1 (2003).
[8] P. Saravanapavan, Larry L. Hench, J. Biomed Mater Res: **54**, 608 (2001).
[9] J. Simitzis, D. E. Baciu, S. Soulis, M. Tzedaki, J. Optoelectron. Adv. Mater. **12**(5), 1213 (2010).
[10] T. Kokubo, H. Kushitani, S. Sukka, T. Kitsugi, T. Yamamuro, J. Biomed. Res. **24,** 721 (1990).
[11] I. Izquierdo- Barba, J. Salinas, M. Vallet- Regi, Journal of Biomedical research **47,** 243 (1999).
[12] M. Vallet-Regi, C. V. Ragel, A. Salinas, Eur. J. Inorg. Chem., p. 1029-1042 (2003).
[13] A. Martinez, I. Izquierdo- Barba, M. Vallet- Regi, Chem. Mater. **12,** 3080 (2000).
[14] J. Zhong, David. C. Greenspan, Journal of Biomedical research **53,** 694 (2000).
[15] S. Padilla, J. Roman, A. Carenas, M. Vallet- Regi, Biomaterials **26**, 475 (2005).
[16] S. Ramesh, K. H. Leen, K. Kumutha, A. K. Arof, Spectrochimica Acta Part A, **66,** 1237 (2007).
[17] C. Parra, Gema Gonzales, C. Albano, e-Polymers, no. **025** (2005).
[18] S. Rajendradan, T. UMA, Bull. Mater. Sci., **23**(1), 27 (2000) ©Indian Academy of Sciences.
[19] D. Arcos, C.V. Ragel, M. Vallet-Regi, Biomaterials **22,** 701 (2001).
[20] H. Takadama, H. M. Kim, T. Kokubo, T. Nakamura, Chem. Mater. **13**, 1108 (2001).
[21] Weam. F. Mousa, M. Kobayashi, S. Shinzato, M. Kamimura, M. Neo, S. Yoshihara, T. Nakamura, Biomaterials **21,** 2137 (2000).

*Corresponding author: dianabaciuro@yahoo.com